Biotechnology for Biofuels

An accurate description of Aspergillus niger organic acid batch fermentation through dynamic metabolic modelling

--Manuscript Draft--

Manuscript Number:	BBIO-D-17-00324
Full Title:	An accurate description of Aspergillus niger organic acid batch fermentation through dynamic metabolic modelling
Article Type:	Research
Section/Category:	Fungal/yeast genetics, physiology and metabolic engineering
Funding Information:	Biotechnology and Biological Sciences Research Council (BB/J014443/1) · Mr Daniel Upton

Abstract:	**Background** Aspergillus niger fermentation has provided the chief source of industrial citric acid for over 50 years. Traditional strain development of this organism was achieved through random mutagenesis, but advances in genomics have enabled development of genome-scale metabolic modelling that can be used to make predictive improvements in fermentation performance. The parent citric acid producing strain of A. niger, ATCC 1015, has been described previously by a genome-scale metabolic model that encapsulates its response to ambient pH. Here, we report the development of a novel double optimisation modelling approach that generates time-dependent citric acid fermentation using dynamic flux balance analysis. **Results** The output from this model shows a good match with empirical fermentation data. Our studies suggest that citric acid production commences upon a switch to phosphate-limited growth and this is validated by fitting to empirical data, which confirms the diauxic growth behaviour and the role of phosphate storage as polyphosphate. **Conclusions** The calibrated time-course model reflects observed metabolic events and generates reliable in silico data for industrially relevant fermentative time series, and for the behaviour of engineered strains suggesting that our approach can be used as a powerful tool for predictive metabolic engineering.

Corresponding Author:	Daniel Upton University of York UNITED KINGDOM
Corresponding Author Secondary Information:	
Corresponding Author's Institution:	University of York
Corresponding Author's Secondary Institution:	
First Author:	Daniel Upton
First Author Secondary Information:	
Order of Authors:	Daniel Upton
	Simon McQueen-Mason
	Andrew Jamie Wood
Order of Authors Secondary Information:	

An accurate description of *Aspergillus niger* organic acid batch fermentation through dynamic metabolic modelling

Daniel J. Upton[1], Simon J. McQueen-Mason[1], A. Jamie Wood[1,2]

Author details:

Author 1: Daniel John Upton

Email address: dju500@york.ac.uk

Author 2: Simon John McQueen-Mason

Email address: simon.mcqueenmason@york.ac.uk

Author 3: Andrew Jamie Wood

Email address: jamie.wood@york.ac.uk

Institutional addresses:

1. Department of Biology, University of York, Wentworth Way, York, YO10 5DD, United Kingdom

2. Department of Mathematics, University of York, Heslington, York, YO10 5DD, United Kingdom

Correspondence to A. Jamie Wood

1

Abstract

Background

Aspergillus niger fermentation has provided the chief source of industrial citric acid for over 50 years. Traditional strain development of this organism was achieved through random mutagenesis, but advances in genomics have enabled development of genome-scale metabolic modelling that can be used to make predictive improvements in fermentation performance. The parent citric acid producing strain of *A. niger*, ATCC 1015, has been described previously by a genome-scale metabolic model that encapsulates its response to ambient pH. Here, we report the development of a novel double optimisation modelling approach that generates time-dependent citric acid fermentation using dynamic flux balance analysis.

Results

The output from this model shows a good match with empirical fermentation data. Our studies suggest that citric acid production commences upon a switch to phosphate-limited growth and this is validated by fitting to empirical data, which confirms the diauxic growth behaviour and the role of phosphate storage as polyphosphate.

Conclusions

The calibrated time-course model reflects observed metabolic events and generates reliable *in silico* data for industrially relevant fermentative time series, and for the behaviour of engineered strains suggesting that our approach can be used as a powerful tool for predictive metabolic engineering.

Keywords: *Aspergillus niger;* citric acid; dFBA; metabolic modelling; polyphosphate

2

Background

Due to its natural ability to secrete organic acids and proteins, the filamentous

fungus *Aspergillus niger* is an established organism for the industrial production of

citric acid and enzymes. *A. niger* is metabolically highly versatile, a feature that has

made it useful for a wide range of biotechnological biotransformations [1]. *A. niger*

also produces a wide range of secondary metabolites, with over 100 reported to date

[2]. *A. niger* is a saprotroph and its natural habitat is soil, although it can be found in

wide-ranging habitats, such as rotting fruit, plant debris, and indoor environments.

This fast-growing fungus is both acid- and thermo-tolerant, able to grow in the pH

range 1.4-9.8 and in the temperature range 6-47ºC [3]. This versatility and its ease of

culture has helped it become an established industrial organism. Its haploid genome

is around 35 Mb in size with 8 chromosomes which contain about 12,000 genes,

57% of which have functional assignments [4]. Aspergilli are an important and

diverse group, which in addition to *A. niger,* include well-studied species such as the

model genetic organism *A. nidulans*, the pathogen *A. fumigatus* and the

domesticated *A. oryzae*. Full genome sequences are currently available for 18

species of the Aspergilli group [5] and some of these have been subject to extensive

systems biology studies [6].

With global production of 2 million tonnes a year, citric acid is an industrial chemical

with many applications [7]. Its main use is in the food and drinks industry, but is also

used in cleaning agents, pharmaceuticals, animal feed, and metal cleaning [8].

Industries using *A. niger* fermentation are dependent on sucrose-based feedstocks,

70 but with rising costs and increasing concerns over food security, a switch to more

71 sustainable and lower cost feedstocks is desirable [9]. *A. niger* can assimilate a wide

72 range of carbon sources, and therefore has great potential for exploiting underused

73 resource streams such as pentose sugars from lignocellulose.

74

75 The best industrial strains are capable of producing over 70% of the theoretical yield

76 of citric acid [10]. Such strains have been developed over many decades by time-

77 consuming random mutagenesis. The genotype of resulting strains remains

78 unknown, and random mutagenesis can lead to genetic instability of developed

79 strains. Rational engineering of *A. niger* is now feasible, particularly with advances in

80 genomics over recent years that have paved the way for genome-scale metabolic

81 modelling [5, 11]. Industrially, *A. niger* is utilised via large-scale batch fermentations

82 rather than continuous culture methods, typically in reactors in excess of 100,000

83 litres [12]. In order for genome-scale models to accurately capture the behaviour of

84 these cultures, techniques which model the batch growth, rather than simple

85 chemostat-like cultures, are required.

86

87 The genome of the parent citric acid producing strain of *A. niger*, ATCC 1015, has

88 been sequenced [4]. This enabled development of the genome-scale metabolic

89 model for *A. niger*, *i*MA871, which reflects ATCC 1015 metabolism [13]. The model

90 was further developed to reflect the well-known behaviour of *A. niger* to acidify its

91 surroundings in response to ambient pH [14]. This was achieved by incorporating

92 acid-dissociation reactions for seven organic acids reportedly secreted by *A. niger*.

4

93 Each reaction gives the number of protons released by a particular acid as a function

94 of ambient pH. Citric acid production was modelled statically using flux balance

95 analysis (FBA). The objective function was either set to proton production at a fixed

96 growth rate or proton production was incorporated into the biomass equation. The

97 nature of organic acid production in response to ambient pH is, however, a dynamic

98 one, with acid-dissociation reactions changing as protons are produced.

99

100 In this article, we further develop the *A. niger* metabolic model to take into account

101 the dynamic nature of organic acid production. By designing a novel modelling

102 approach that employs dynamic flux balance analysis (dFBA), we demonstrate a

103 model that gives time-course fermentative series of citric acid production. We

104 validate the new model by fitting to empirical data from ATCC 1015 citric acid

105 fermentations, and demonstrate how the resultant time-course calibrated model can

106 be used as a powerful platform for metabolic engineering of *A. niger*.

107

Results

Citric acid fermentation occurs as part of a diauxic growth response

110 To investigate citric acid production by the parent citric acid producing ATCC 1015

111 strain, empirical time course data were obtained from fermentation performed in

112 shake flasks. Biomass and citric acid production were monitored with samples taken

113 at 24 hour time-points. Diauxic growth behaviour was observed, with a drop in

114 growth rate at day 3 (Fig 1A). Citric acid production commenced at day 3, coinciding

115 with the diauxic growth shift (Fig 1B). 60 g/L citric acid was produced.

116

117 In order to better understand the basis of this growth behaviour we developed a

118 dynamic flux balance analysis (dFBA) model based on the previously published FBA

119 model [13, 14]. To validate the model and further investigate the diauxic growth

120 behaviour, empirical data were obtained for citric acid fermentation under a range of

121 phosphate levels (0.05, 0.09 and 0.17 g/L). Samples of the cultures were taken

122 every 24 hours to produce a time-course of biomass dry weight, phosphate

123 depletion, citric acid production, and glucose consumption (Fig 2). Phosphate was

124 rapidly taken up and depleted by day 2 (Fig 2B), yet growth continued (Fig 2A).

125 Phosphate was therefore clearly stored internally to enable growth during absence of

126 external phosphate. Diauxic growth was observed, with growth becoming phosphate-

127 limited. The diauxic growth shift was synchronous with depletion of external

128 phosphate. The phosphate-limited growth rate was a function of the initial phosphate

129 concentration, with increased growth rate at higher phosphate. The timing of citric

130 acid production was observed to coincide with the onset of phosphate-limited growth

131 and external phosphate depletion (Fig 2C). Up to 50 g/L citric acid was produced,

132 with the culture at 0.17 g/L phosphate producing the most. Glucose uptake was

133 relatively slow for the lower phosphate cultures and a limiting factor in citric acid

134 production (Fig 2D).

135

136 From these observations, we hypothesised that the diauxic growth shift is caused by

137 a switch to phosphate-limited growth, resulting in citric acid production. This

138 hypothesis was motivated by examination of our data, existing knowledge of *A. niger*

6

139 [10] and also the ecological evidence that organic acids are released extracellularly

140 in order to facilitate the mobilisation of phosphate, especially in soil [15]. We decided

141 to examine the plausibility of this hypothesis using dFBA modelling.

142

Simulating citric acid fermentation by dynamic flux balance analysis

144 To create time-course simulations comparable to the citric acid fermentation

145 empirical data, dynamic flux balance analysis (dFBA) was used with the _i_MA871

146 metabolic model [13]. Citric acid production was modelled by incorporating kinetic

147 acid-dissociation reactions into the dFBA schema for the organic acids in _i_MA871

148 and setting the objective to proton production. This explicit inclusion leads to an acid

149 hierarchy [14], which suggested that citric acid production was the most efficient

150 means of acidification with oxalic acid production switched off.

151

152 In the standard setting for the metabolic model citric acid secretion is included as a

153 part of the external constraints during growth [13]; however, this is not supported by

154 our observations. Therefore, a novel modelling approach was designed to simulate

155 the diauxic growth behaviour with citric acid production commencing upon a diauxic

156 growth shift coupled to phosphate intake. To achieve this, a double optimisation

157 dFBA setup was designed (Fig 3). The objective is first set to biomass production,

158 with the maximised growth rate then used in the second optimisation. The second

159 objective is dependent on the growth-limiting condition of the first optimisation. The

160 decision process uses a boolean expression. If the external phosphate flux is lower

161 than its flux constraint, the second objective is set to phosphate storage to store

162 excess phosphate not used for growth. Otherwise, external phosphate flux is equal

163 to its flux constraint and the second objective is set to proton production to make use

164 of the carbon not used for growth (phosphate-limited growth).

165

166 The dynamic modelling approach, dFBA, therefore includes a number of metabolite

167 pools that are tracked outside of the FBA, including external glucose, external

168 phosphate, external pH, organic acids as well as the hypothesised stored phosphate.

169 These metabolite pools are linked to the FBA simulations at each step via first order

170 differential equations describing transport processes. These differential equations

171 are solved at each time-step to provide flux constraints for the FBA optimisations

172 occurring in a tandem fashion and assuming the metabolic system remains at a

173 steady-state despite the small changes in the external constraints. All equations

174 used are detailed in the methods, but are essentially either linear diffusion or

175 Michaelis-Menten transport equations across the membrane as described below and

176 mathematically in the methods section. Literature sources were used to

177 parameterise the model wherever available as described below.

178

179 Following previous studies [16, 17], glucose uptake was modelled as the sum of

180 passive diffusion and facilitated diffusion, using empirical values from the literature

181 [16, 17] for all transport-mediated kinetic parameters (Table 2). The calculated

182 parameter for passive diffusion overestimated glucose uptake, and therefore was

183 fitted to empirical data (Table 1). Transport-mediated glucose uptake in *A. niger* is

184 inhibited by low pH and non-competitively inhibited by external citrate [17], and this

8

185 was therefore included in the modelled glucose uptake. *A. niger* has both low- and

186 high-affinity glucose transport systems [17], both of which were included in the

187 model. The low-affinity system is reported only active above 150 g/L glucose, [17]

188 and so this system was only included in the model at high glucose (>150 g/L).

189

190 Phosphate uptake and release of stored phosphate were modelled according to

191 Michaelis-Menten kinetics. As no characterised phosphate transporters could be

192 found for *A. niger* in the literature, kinetic parameters were fitted to empirical data on

193 phosphate uptake (Table 1).

194

Fitting of model parameters to empirical data and model validation

196 The empirical data obtained from the experiment varying phosphate were used to fit

197 model parameters and validate the model. A total of eight parameters were fitted to a

198 data-set containing 84 data-points. As each data-point was in quadruplicate with very

199 low error margins, we decided to use the data-set for both model training and

200 validation. The trained model was later applied to independent data-sets (Fig 4),

201 which gave further validation. Using the trained model, citric acid fermentation was

202 simulated for each of the phosphate levels tested, and model predictions plotted

203 alongside empirical data (Fig 2). The modelled diauxic growth behaviour gave good

204 fits to empirical data, with external phosphate depletion being the trigger that results

205 in phosphate-limited growth and citric acid production. All the model outputs showed

206 a strong qualitative comparison to the empirical data with unfitted parameters taken

207 directly from the literature. Notably the modelled glucose uptake fitted empirical data

9

208 closely (Fig 2D) with unadjusted literature values for transport-mediated uptake rate

209 and affinity.

210

211 However, a number of adjustments were required for the model to fit the empirical

212 data more closely. In particular, the model underestimated biomass production

213 during phosphate-limited growth, suggesting a lower phosphate demand not

214 reflected in the *i*MA871 biomass equation. These contrasting observations in the

215 different areas of growth suggest that the biomass equation for the *i*MA871 model

216 represents an average biomass composition over different growth conditions and

217 that therefore the biomass equation needs to be altered. Differences in biomass

218 composition in different growth conditions have previously been reported in

219 *Escherichia coli* [18]. To reflect citric acid producing conditions, two new fitted

220 parameters were added to the model, the nucleic acid and phospholipid components

221 of the biomass equation (Supplementary Table S1). The ratios between the different

222 components of each, and the total mass of the biomass components were kept

223 constant. Change in mass was balanced by adjustment of the glycerol component,

224 which has been reported to increase during citric acid producing conditions [19]. The

225 additional parameters increase the complexity of the model, and the likelihood of

226 overfitting. Therefore, Akaike Information Criterion (AIC) [20] was used to measure

227 the quality of fit and assess improvement in the model (Table 4) (see Methods).

228

229 Our model initially overestimated citric acid production. This may be due to the many

230 internal constraints imposed on the internal metabolism by the intracellular

10

231 accumulation of, or simply high throughputs of citrate that are not accounted for by

232 the steady-state methodology of flux balance analysis. For example, the citrate

233 sensitivity of 6-phosphofructo-1-kinase is a target of attempts to increase citrate

234 production [21] and the rates of mitochondrial citrate export [22] and citrate secretion

235 may be limiting. To reflect these constraints a limit to the citric acid output rate, v_{CIT},

236 was added and fitted as a parameter to more closely reflect empirical data (Table 1).

237 Carbon uptake was decreased slightly as a result of the constraint on citric acid

238 output, but still gave close fits to empirical data. The new model was assessed by

239 calculating the AIC (see Methods), which showed a significant improvement (Table

240 4).

241

Citric acid production on other carbon sources

243 To further investigate the diauxic growth behaviour, we tested citric acid fermentation

244 using D-xylose as a substrate at an initial concentration of 160 g/L. The same diauxic

245 growth shift coupled citric acid response was seen with xylose (Fig 4) as seen with

246 glucose. We applied our model, with previously fitted parameters unchanged. The

247 empirical data from this experiment was not used in previous model training, and

248 served to provide further validation with glucose as substrate and at a different

249 phosphate level. The uptake rate of xylose was modelled similarly to glucose as the

250 sum of passive and facilitated diffusion. The kinetic parameters for xylose uptake

251 were fitted to our empirical data (Table 1). Close fits were achieved for biomass

252 production and carbon source consumption, demonstrating the wide applicability of

253 the dynamic model. Citric acid production was overestimated by the model, which

11

254 may suggest a further limiting factor with xylose as the carbon source. The constraint

255 applied to citric acid output rate, v_{CIT}, was the same as for glucose (Table 1). The

256 discrepancy may be due to differing morphology as we observed decreased biomass

257 pellet sizes and higher viscosity in cultures grown on xylose.

258

Investigating the role of phosphate during citric acid fermentation

260 As growth on glucose continued beyond external phosphate depletion (Fig 2B), it

261 became clear that *A. niger* has a phosphate storage mechanism, possibly via

262 accumulation of polyphosphate as previously reported [23]. To investigate this,

263 polyphosphate was extracted from biomass grown under citric acid producing

264 conditions and quantified. Polyphosphate levels were observed to rise early on in

265 fermentation, peaking at day 2 at the point of external phosphate depletion (Fig 5).

266 Polyphosphate levels dropped rapidly from day 2 to day 4, with a more gradual

267 decrease later in fermentation coinciding with phosphate-limited growth and citric

268 acid production.

269

270 To further investigate the importance of phosphate, we searched for the genes

271 encoding phosphate transporters in *A. niger* ATCC 1015. A total of 8 putative genes

272 were found (based on similarity to known transporters), suggesting *A. niger* has

273 evolved a range of phosphate uptake mechanisms as adaptation to different

274 environmental conditions (Supplementary Table S2). It may be that only a subset of

275 these genes encode phosphate transporters while others encode phosphate

276 sensors. One of the genes (accession number EHA22558) has clear homologues in

12

277 other species (Fig S1), but none of these have been characterised or parameterised

278 at the level of protein activity. The other gene annotations are more speculative so

279 may not encode phosphate transporters [24].

280

The dFBA model provides a platform for predictive metabolic engineering

282 A prediction of the model is that oxalic acid production is the most efficient means of

283 acidification at initial pH 7, followed by citric acid. It is well known that *A. niger*

284 predominantly secretes oxalic and gluconic acid at higher initial pH and that by

285 imposing a low initial pH during fermentation, production of these competing organic

286 acids is prevented and citric acid production is increased [14]. Our model suggests

287 that by switching off oxalic acid production by deletion of oxaloacetate hydrolase

288 (oah), citric acid will solely be produced. The model does not predict gluconic acid

289 production suggesting this may be decoupled from proton production and is instead

290 a means of quickly sequestering glucose, through the action of extracellular glucose

291 oxidase, early in fermentation.

292

293 To investigate this phenomenon, we engineered the ATCC 1015 strain by targeted

294 gene deletion strategies to knockout oah and the gene encoding glucose oxidase

295 (gox) responsible for gluconic acid production. We created two single knockouts

296 (Δoah and Δgox) and a double knockout (Δoah Δgox), and characterised citric acid

297 fermentation by these knockout strains at initial pH 7 (Fig 6). Citric acid yield was

298 significantly increased in the Δoah strain with a further marginal improvement in

299 Δoah Δgox. This was not the case for the Δgox strain suggesting gluconic acid

13

300   production occurs independently of proton production without impacting citric acid

301   fermentation. Gluconic acid was produced early in fermentation while oxalic and

302   citric acid production occurred later. The synchronicity of oxalic and citric acid

303   production suggests they are part of the same proton production response. In this

304   experiment, the Mn^{2+} concentration was increased to 1000 ppb. Citric acid

305   production usually requires Mn^{2+}-deficient media, though was previously reported

306   insensitive to Mn^{2+} in an oah and gox double negative mutant strain at pH 5 [25]. The

307   presence of Mn^{2+} did not prevent citric acid production at initial pH 7, suggesting that

308   its effect is limited to low pH conditions.

309

310   We applied our dFBA model to the Δoah and Δgox knockouts at initial pH 7, which

311   gave close fits for oxalic and gluconic production. The differences in predicted citric

312   acid production between the knockout strains showed a qualitative fit with empirical

313   data (Fig 6). However, constraints on oxalic and citric acid output rates, v_{OXAL} and

314   v_{CIT} respectively (Table 1), were required to achieve the close fits. The constraint on

315   citric acid output rate, v_{CIT}, was different to that applied at initial pH 2. This may be

316   due to morphological differences as we observed increased biomass pellet sizes

317   when *A. niger* was grown at higher initial pH. The impact of differing morphology on

318   transport processes and on anaerobicity within pellets requires further investigation.

319   The widely reported absence of oxalic acid production below pH 2 [10, 25] was

320   implemented in the model to reflect empirical data. To simulate gluconic acid

321   production, the flux of the extracellular GOX and gluconic acid dissociation reactions

322   were forced dependent on GOX kinetic parameters and the ambient pH. The kinetic

323 parameters V_{max} and K_M of GOX (Table 2) were taken from the literature [26, 27].

324 The concentration of GOX per gram biomass dry weight is unknown for these

325 experimental conditions so was fitted to empirical data (Table 1). The proportion of

326 active GOX was based on empirical data of GOX activity at varying pH [28].

327

Discussion

329 We have developed a novel dynamic model of *A. niger* citric acid fermentation that

330 employs dFBA, to give time-course simulations of batch fermentation relevant to the

331 industrial and experimental modes of *A. niger* fermentation. Our physiologically

332 motivated double optimisation approach is a novel use of dFBA. Previous work

333 incorporated proton production into the *i*MA871 metabolic model and used FBA in a

334 static manner to give predictions on organic acid production [13, 14] at fixed values

335 of pH. Since acid dissociation reactions are dependent on the dynamic ambient pH,

336 the application of dFBA with the dynamic tracking of pH enables more accurate

337 predictions on organic acid production. The dynamic model was also expanded to

338 include alternative feedstocks. Xylose was chosen as it is a pentose sugar abundant

339 in hemicellulose in plant biomass and readily metabolised by *A. niger*. This new

340 dynamic model is therefore a valuable addition to the *A. niger* metabolic modelling

341 toolbox and a powerful demonstration of the promise of dFBA for applications in

342 industrial biotechnology.

343

344 We tested the ability of the model to predict the impact of genetic modifications on

345 organic acid fermentation at higher initial pH. We deleted genes encoding

15

346 oxaloacetate acetylhydrolase (oah) and glucose oxidase (gox) to eliminate oxalic

347 and gluconic production respectively. Deletion of oah significantly increased citric

348 acid production, and this was also observed in model predictions, though less

349 pronounced. This suggests that the presence of oxalic acid in the cytosol in the oah

350 positive strains may have negating effects on citric acid production not reflected by

351 the model. It is expected that cytosolic organic acid accumulation may occur as a

352 result of constrained transport, which is likely to have regulatory effects on organic

353 acid production as a safeguard mechanism.

354

355 *A. niger* has been an industrial workhorse for decades and is essential to the world's

356 citric acid production. This is achieved through batch or fed-batch fermentation and

357 the new model enables simulation of the dynamic process for the first time. The

358 underlying causes of the naturally evolved property of organic acid production are

359 still unclear. It was previously reported through static FBA predictions [14] that this

360 may be driven by the biological objective of proton production. In line with empirical

361 findings, oxalic acid production was revealed as the most efficient means of proton

362 production at wide ranging pH with citric acid second at low pH. We have now shown

363 this in a dynamic manner with variable external pH taken into account. Empirical

364 data revealed that oxalic and citric acid production are synchronous upon a switch to

365 phosphate-limited growth. This suggests they are coupled and part of the same

366 proton production response. This is further supported by the significant increase in

367 citric acid production in Δoah.

368

16

369 The role of phosphate is striking as organic acid secretion has been reported in *A.*

370 *niger* and other organisms as a phosphate mobilisation strategy [15, 29, 30]. The

371 observed phosphate-limited growth results from the ability of *A. niger* to rapidly take

372 up phosphate and store it as polyphosphate. The constraint on polyphosphate

373 hydrolysis then limits growth, enabling flux of carbon to organic acid production.

374 While *A. niger* has sufficient stored phosphate for growth, it does not use it and

375 keeps it reserved. This behaviour may be due to the energy storage value of

376 polyphosphate. We have observed a release of phosphate late in fermentation upon

377 carbon depletion, which suggests *A. niger* is capable of rapid polyphosphate

378 hydrolysis as a means to create ATP when other energy sources are limiting. The

379 control mechanisms that exist in *A. niger* to regulate polyphosphate hydrolysis and

380 their relation to organic acid production warrant further investigation.

381

382 Our modelling approach has further demonstrated the potential of dFBA; the

383 augmentation of static steady state FBA by dynamic transport processes and time

384 varying pools of metabolites. It has also revealed some fundamental issues with the

385 application of these techniques to real applications. The objective function – the

386 biomass equation – is fundamental to FBA and is typically constructed with evidence

387 from mass spectrometry. Our work suggests that this function is strongly dependent

388 on the fermentation context and may even be variable over the growth process.

389 Biologically this is highly plausible, but dramatically increases the complexity of

390 model implementation and fitting. In addition, it is clear that important regulatory

391 constraints on the metabolic process, in this case citrate accumulation, need to be

17

392 included. In this manner, we have created an augmented dFBA model in a

393 potentially grey area between a complete kinetic model and the genetically based

394 simplicity of an FBA model. Further work is required to fully understand validity of

395 such models.

396

Conclusions

398 Our findings reveal a naturally evolved behaviour that has been exploited by industry

399 for decades to produce citric acid. Our work, encapsulated in a dynamic model,

400 further elucidates the causative factors in organic acid fermentation by *A. niger*

401 exploited by industrial processes. The model provides a means to further probe this

402 behaviour and accurately explore the effects of genetic changes on organic acid

403 fermentation in a dynamic manner. This new addition to the *A. niger* systems biology

404 toolbox paves the way for metabolic engineering efforts to create new strains

405 capable of enhanced citric acid production on low-cost feedstocks.

406

Methods

Shake flask experiments

409 Citric acid fermentation experiments were performed in 250 ml DeLong neck baffled

410 shake flasks (Bellco Glass Inc.; Vineland, NJ, USA) with 30 ml medium. Flasks were

411 siliconized with 2% (v/v) dimethyldichlorosilane. Cultures were incubated at 30ºC

412 with shaking at 250 rpm. The following medium was used: glucose (160 g/L), urea

413 (3.6 g/L), $(NH_4)_2SO_4$ (0.52 g/L), K_2HPO_4 (0.5 g/L), $CaCO_3$ (0.03125 g/L),

414 $MgSO_4.7H_2O$ (0.275 g/L), $ZnSO_4.7H_2O$ (0.00225 g/L), $FeSO_4.7H_2O$ (0.0095 g/L),

18

415    $CuSO_4.5H_2O$ (0.0117 g/L), $MnCl_2.(H_2O)_4$ (0.0000108 g/L), citric acid monohydrate

416   (3.3 g/L), Tween 80 (0.0094%). The Mn^{2+} concentration was confirmed as 7 ppb by

417   ICP-MS (Biorenewables Development Centre, York, UK). The medium was

418   autoclaved (121ºC 15 minutes) excluding glucose which was filter sterilised (0.22

419   μm). The pH of the medium was adjusted after autoclaving by addition of sterile 2 M

420   H_2SO_4. The medium included 10 mM uridine in experiments using pyrG negative

421   strains. The medium was inoculated with 1×10^6 spores/ml. Spores were harvested

422   from potato dextrose agar slants incubated for 2 days at 37ºC. 2 ml saline Tween

423   (0.1% Tween 80, 9 g/L NaCl) was added per slant and shaken to disperse spores.

424   Spores were washed 3 times in saline Tween. 500 μl samples of cultures were taken

425   every 24 hours for determination of biomass, metabolites and phosphate. Samples

426   were collected in pre-dried, pre-weighed 1.5 ml Eppendorf tubes and centrifuged at

427   9000 g for 5 minutes. The supernatant was retained for metabolite analysis and

428   phosphate determination and stored at -20ºC.

429

430   **Biomass dry weight determination**

431   Mycelia were washed 4 times in 1 ml dH_2O and centrifuged at 9000 g for 5 minutes.

432   Biomass was dried at 70ºC to constant weight. Biomass dry weight was determined

433   by subtracting weight of the pre-dried 1.5 ml Eppendorf tube.

434

435   **Metabolite analysis**

436   Enzymatic assay kits were used to determine the level of metabolites. Glucose, citric

437   acid, xylose, glycerol and gluconic acid were determined using Megazyme assay kits

19

438 (K-GLUC, K-CITR, K-XYLOSE, K-GCROLGK, and K-GATE respectively)

439 (Megazyme International Ireland Ltd., Wicklow, Ireland). Oxalic acid was determined

440 using the LIBIOS oxalate assay kit (Oxalate-100; LIBIOS, France).

441

Phosphate determination

443 Phosphate was determined by the ammonium molybdate method, using an assay kit

444 (ab65622; Abcam, Cambridge, UK).

445

Polyphosphate extraction and quantification

447 Mycelia were grown up in shake flasks using the same method as previously

448 described. Mycelia were harvested at 8 time-points (days 1 to 8) in triplicate. To

449 obtain sufficient biomass, one flask was harvested per sample. Day 1 samples

450 required the pooling of 4 flasks per replicate. Mycelia were harvested using a double

451 layer of Miracloth (Calbiochem) and washed in 300 ml ice-cold 100 mM Tris.HCl pH

452 7 followed by 600 ml ice-cold dH_2O. Washed mycelia were transferred to 15 ml

453 Falcon tubes, flash frozen in liquid nitrogen, freeze dried, and stored at -80ºC.

454 Freeze dried mycelia were weighed out in 2 ml vials, approximately 50 mg per vial.

455 Biomass was ground using the TissueLyser II (QIAGEN; Crawley, UK) at 30 Hz for

456 90 seconds 3 times. Each vial contained 2 beads. Powdered mycelia were lysed by

457 adding 2 ml 10% (w/v) lysing enzymes from *Trichoderma harzianum* (Sigma, Dorset,

458 UK) and incubating at 30ºC with shaking for 3 hours. Samples were centrifuged and

459 supernatant discarded. Polyphosphate was extracted following a previously

460 described protocol [23]. All centrifuge steps were done at 13,000 rpm for 10 minutes

20

461 at 4ºC and all shaking was done at 30 rpm. The polyphosphate fraction was dried in

462 a Savant SPD131DDA SpeedVac Concentrator (Thermo Fisher Scientific).

463 Polyphosphate was quantified by measuring free phosphate before and after acid

464 hydrolysis using the previously described phosphate determination method. Acid

465 hydrolysis was performed by adding 2 ml 0.5 M H_2SO_4 to the dry pellet and boiling at

466 100ºC for 3 hours.

467

Dynamic modelling of organic acid fermentation

469 Modelling was performed using the *i*MA871 metabolic model [13] as the model for

470 the flux balance analysis. During this project, a more complete model of *A. niger*

471 metabolism was published [31] but as this retains the core of *i*MA871 and is not

472 specific to ATCC 1015 we have not adopted this model. The FBA calculations were

473 performed using bespoke Java code which implements the GLPK toolkit (GNU).

474 dFBA routines were written directly into the Java code with the differential equations

475 solved by simple time-stepping (Euler method) with small values for the time-step.

476 The ODEs (ordinary differential equations) were solved according to

$$C_{n+1} = C_n + t f_n B_n, \tag{1}$$

478 where C_{n+1} is the mmol of compound at time-point n+1, C_n is the mmol of compound

479 at time-point n, t is the time-step (1/60 h), f_n is the flux (mmol gDW^{-1} h^{-1}) at time-

480 point n, and B_n is the biomass (gDW) at time-point n. The flux constraints at time-

481 point n+1 were calculated by the following kinetic equations. External phosphate

482 input (PIe<==>) was constrained according to

$$v_{Pe} = \frac{v_{Pe,max} P_e}{K_{Pe} + P_e}, \tag{2}$$

21

484   where v_{Pe} is the external phosphate uptake rate (mmol gDW^{-1} h^{-1}) and P_e is the

485   external phosphate concentration (mM).

486   Internal phosphate input (PI<==>) was constrained according to

487 $$v_P = \frac{v_{P,max}P}{K_P + P},$$ (3)

488   where v_P is the internal phosphate input rate (mmol gDW^{-1} h^{-1}) and P is the

489   concentration of stored phosphate (mM).

490

491   If external glucose was below 150 g/L, external glucose uptake (DGLCe<==>DGLC)

492   was constrained according to

493 $$v_G = v_{G1}G + \frac{v_{G2,max}G}{K_{G2}\left(1+\frac{C}{K_{i2}}\right)+G\left(1+\frac{C}{K_{i2}}\right)},$$ (4)

494   where v_G is the external glucose uptake rate (mmol gDW^{-1} h^{-1}), G is the external

495   glucose concentration (mM), and C is the external citrate concentration (mM).

496   If external glucose was greater than or equal to 150 g/L, external glucose uptake

497   was constrained according to

498 $$v_G = v_{G1}G + \frac{v_{G2,max}G}{K_{G2}\left(1+\frac{C}{K_{i2}}\right)+G\left(1+\frac{C}{K_{i2}}\right)} + \frac{v_{G3,max}G}{K_{G3}\left(1+\frac{C}{K_{i3}}\right)+G\left(1+\frac{C}{K_{i3}}\right)},$$ (5)

499   where v_G is the external glucose uptake rate (mmol gDW^{-1} h^{-1}), G is the external

500   glucose concentration (mM), and C is the external citrate concentration (mM).

501   If external xylose was below 150 g/L, external xylose uptake (XYLe<==>) was

502   constrained according to

503 $$v_X = v_{X1}X + \frac{v_{X2,max}X}{K_{X2} + X},$$

504 (6)

22

505 where v_X is the external xylose uptake rate (mmol gDW^{-1} h^{-1}), and X is the external

506 xylose concentration (mM).

507 If external xylose was greater than or equal to 150 g/L, external xylose uptake was

508 constrained according to

$$v_X = v_{X1}X + \frac{v_{X2,max}X}{K_{X2}+X} + \frac{v_{X3,max}X}{K_{X3}+X}, \tag{7}$$

510 where v_X is the external xylose uptake rate (mmol gDW^{-1} h^{-1}), and X is the external

511 xylose concentration (mM).

512 The extracellular GOX (glucose oxidase) reaction rate was calculated according to,

$$v_{GOX} = p_{GOX}\frac{v_{GOX,max}G}{K_{GOX}+G}, \tag{8}$$

514 where v_{GOX} is the GOX reaction rate, p_{GOX} is the proportion of active GOX, and G is

515 the external glucose concentration (mM).

516 The proportion of active GOX, p_{GOX}, as a function of pH was determined according

517 to,

$$p_{GOX} = -0.102pH^2 + 1.082pH - 1.95 \tag{9}$$

519 The kinetic parameters were either fitted to our empirical data (Table 1) or set to

520 empirical values from the literature if available (Table 2).

521

522 The *i*MA871 model was adapted to include proton production as an objective

523 function and acid-dissociation reactions for seven acids (citric, oxalic, gluconic,

524 acetic, malic, succinic, lactic) but as a function of a dynamic external pH rather than

525 a fixed pH [14]. The number of protons released in each acid-dissociation reaction

526 was calculated at each time-step according to the following equation based on

527 ambient pH and pKa values.

23

$$H = \frac{K_1(H_e)^{-1} + 2K_1K_2(H_e)^{-2} + 3K_1K_2K_3(H_e)^{-3}}{1 + K_1(H_e)^{-1} + K_1K_2(H_e)^{-2} + K_1K_2K_3(H_e)^{-3}}, \tag{10}$$

528

529 where K_1, K_2, and K_3 are constants calculated from pKa values of each acid species

530 (Table 3), and H_e is the external molar concentration of protons that is tracked in the

531 dFBA as a dynamic pool.

532

533 An output reaction was added for external protons (Hpe<==>), which was set as the

534 objective when maximising proton production. An explicit phosphate storage reaction

535 was also included in the dFBA. An input reaction for internal phosphate (PI<==>)

536 was added to the metabolic model, and the dynamic pool of internal phosphate was

537 tracked in the dFBA. This new reaction was set as the objective when maximising

538 phosphate storage.

539

540 When plotting alongside empirical data, the dFBA start time was taken as the spore

541 germination time, 18 hours after inoculation. The initial biomass dry weight was set

542 to 0.3125 g/L following empirical data.

543

Model parameterisation

545 Glucose transport-mediated uptake [16, 17] and glucose oxidase [26, 27] kinetic

546 parameters were calculated from empirical data in the literature (Table 2). The

547 concentration of active GOX enzyme [GOX] was fitted to empirical data (Table 1).

548 The other kinetic parameters in the model were fitted to empirical data via a manual

549 fitting routine (Table 1).

550

24

Quality of fit assessment and model selection

Akaike Information Criterion (AIC) [20] was used to measure the quality of fit and

assess improvement in the model. The AIC was calculated according to

$$AIC = 2k + nln\left(\frac{RSS}{n}\right),$$

(11)

where k is the number of fitted parameters, n is the number of data-points, and RSS

is the residual sum of squares.

Targeted gene deletion of oah and gox

Targeted gene deletion was performed using a previously reported strategy [32]. As

this technique requires a pyrG negative strain, the pyrG gene first had to be deleted

from ATCC 1015. This was achieved using homologous recombination. ATCC 1015

was transformed with linear DNA containing 2 kb up- and 1.5 kb down-stream

flanking regions of the pyrG gene (accession number EHA25155), kindly given by M

Kokolski (University of Nottingham). Polyethylene glycol (PEG)-mediated

transformation of protoplasts was used [32]. Successful deletions were selected by

resistance to 5-fluoroorotic acid (5-FOA) (Fluorochem; Derbyshire, UK) and uridine

auxotrophy, and confirmed by PCR and DNA sequencing using primers external to

the gene (pyrG_ex_fw and pyrG_ex_rv). The oah and gox genes were identified in

the ATCC 1015 genome as accession numbers EHA22250 and EHA27180,

respectively. 1.5 kb up- and down-stream flanking regions were cloned from ATCC

1015 gDNA using Phusion HF DNA polymerase (Thermo Fisher Scientific), and the

following primers: oah_up_fw, oah_up_rv, oah_down_fw, oah_down_rv, gox_up_fw,

25

574 gox_up_rv, gox_down_fw, gox_down_rv. 15-bp tails (underlined) were added to

575 outermost primers for In-Fusion® HD cloning (Clontech; France) into the pc3 vector

576 between the NotI and SpeI restriction sites. To join up- and down-stream fragments

577 together, overlap extension PCR was used with 30-bp overlapping tails (underlined)

578 added to innermost primers. Overlapping fragments were first annealed as follows:

579 50 µl reaction containing 200 ng each fragment, 400 µM dNTPs, HF buffer, and 1 U

580 Phusion HF DNA polymerase run on SOE1 programme (94ºC 5 minutes, then 94ºC

581 30 seconds, 60ºC 90 seconds, 72 ºC 90 seconds 10 times, then 10 ºC forever). The

582 annealed product was then amplified using outermost primers as follows: 100 µl

583 reaction containing 50 µl first reaction, 1 µM each primer, 400 µM dNTPs, HF buffer

584 and 1 U Phusion HF DNA polymerase run on SOE2 programme (94ºC 2 minutes,

585 then 94ºC 30 seconds, 60ºC 30 seconds, 72ºC 90 seconds 35 times, then 72ºC 10

586 minutes, 10ºC forever). The annealed product was gel purified using the QIAquick

587 gel extraction kit (QIAGEN; Crawley, UK). Transformation was performed using

588 XL10-Gold Ultracompetent cells according to the manufacturer's instructions (Agilent

589 Technologies; Cheshire, UK). Plasmid was isolated using the Wizard® Plus SV

590 minipreps DNA purification kit (Promega; Southampton, UK). Plasmid integrity was

591 confirmed by DNA sequencing. ATCC 1015 ΔpyrG was transformed with the pc3-

592 oah and pc3-gox deletion vectors using the previously reported PEG-mediated

593 protoplast transformation protocol [32]. The gene deletion procedure previously

594 outlined [32] was then followed with minor modifications. 1.5 g/L 5-FOA was used to

595 select for pyrG negative colonies with incubation at 37ºC for 3 days. oah and gox

596 knockouts were identified by PCR screening with primers external and internal to the

26

597 deletion site (oah_ex_fw, oah_ex_rv, oah_int_fw, oah_int_rv, gox_ex_fw, gox_ev_rv,

598 gox_int_fw, gox_int_rv). Gene deletion was further confirmed by DNA sequencing of

599 the region external to the deletion site. To create the Δoah Δgox double knockout,

600 the deletion procedure for gox was applied to ATCC 1015 ΔpyrG Δoah.

601

Declarations

Ethics approval and consent to participate

604 Not applicable.

Consent for publication

606 Not applicable.

Availability of data and material

608 The datasets used and/or analysed during the current study are available from the

609 corresponding author on reasonable request.

Competing interests

611 The authors declare that they have no competing interests.

Funding

Authors' contributions

615 DJU, AJW and SMM wrote the manuscript. All authors read and approved the final

616 manuscript.

Acknowledgements

618 Not applicable.

References

1. Parshikov IA, Woodling KA, Sutherland JB. Biotransformations of organic compounds mediated by cultures of *Aspergillus niger*. Appl Microbiol Biot. 2015;99:6971-86.

2. Nielsen KF, Mogensen JM, Johansen M, Larsen TO, Frisvad JC. Review of secondary metabolites and mycotoxins from the *Aspergillus niger* group. Anal Bioanal Chem. 2009;395:1225-42.

3. Schuster E, Dunn-Coleman N, Frisvad JC, Van Dijck P. On the safety of *Aspergillus niger*–a review. Appl Microbiol Biot. 2002;59:426-35.

4. Andersen MR, Salazar MP, Schaap PJ, van de Vondervoort PJI, Culley D, Thykaer J, et al. Comparative genomics of citric-acid-producing *Aspergillus niger* ATCC 1015 versus enzyme-producing CBS 513.88. Genome Res. 2011;21:885-897.

5. Cerqueira GC, Arnaud MB, Inglis DO, Skrzypek MS, Binkley G, Simison M, Miyasato SR, Binkley J, Orvis J, Shah P, Wymore F. The *Aspergillus* Genome Database: multispecies curation and incorporation of RNA-Seq data to improve structural gene annotations. Nucleic Acids Res. 2014;42:705-710.

6. Knuf C, Nielsen J. Aspergilli: systems biology and industrial applications. Biotechnol J. 2012;7:1147-55.

7. Chinese citric acid industry begins to consolidate. In: Analysis. F.O. Licht Renewable Chemicals. 2011. http://stage.renewablechemicals.agra-net.com/chinese-citric-acid-industry-begins-to-consolidate/. Accessed 6 July 2017.

28

640   8. Citric Acid. In: Chemical Economics Handbook. IHS. 2015.

641   https://www.ihs.com/products/citric-acid-chemical-economics-handbook.html.

642   Accessed 6 July 2017.

643   9. Dhillon GS, Brar SK, Kaur S, Verma M. Screening of agro- industrial wastes for

644   citric acid bioproduction by *Aspergillus niger* NRRL 2001 through solid state

645   fermentation. J Sci Food Agr. 2013;93:1560-1567.

646   10. Papagianni M. Advances in citric acid fermentation by *Aspergillus niger*:

647   Biochemical aspects, membrane transport and modeling. Biotechnol Adv.

648   2007;25:244-63.

649   11. Orth JD, Thiele I, Palsson BØ. What is flux balance analysis? Nat Biotechnol.

650   2010;28:245-8.

651   12. Max B, Salgado JM, Rodríguez N, Cortés S, Converti A, Domínguez JM.

652   Biotechnological production of citric acid. Braz J Microbiol. 2010;41:862-75.

653   13. Andersen MR, Nielsen ML, Nielsen J. Metabolic model integration of the

654   bibliome, genome, metabolome and reactome of *Aspergillus niger*. Mol Syst Biol.

655   2008;4:178.

656   14. Andersen MR, Lehmann L, Nielsen J. Systemic analysis of the response of

657   *Aspergillus niger* to ambient pH. Genome Biol. 2009;10:R47.

658   15. Schneider KD, Van Straaten P, Orduña D, Mira R, Glasauer S, Trevors J, Fallow

659   D, Smith PS. Comparing phosphorus mobilization strategies using *Aspergillus niger*

660   for the mineral dissolution of three phosphate rocks. J Appl Microbiol. 2010;108:366-

661   74.

662 16. Torres NV, Riol-Cimas JM, Wolschek M, Kubicek CP. Glucose transport by

663 *Aspergillus niger*: the low-affinity carrier is only formed during growth on high glucose

664 concentrations. Appl Microbiol Biot. 1996;44:790-4.

665 17. Papagianni M, Mattey M. Modeling the mechanisms of glucose transport through

666 the cell membrane of *Aspergillus niger* in submerged citric acid fermentation

667 processes. Biochem Eng J. 2004;20:7-12.

668 18. Gonzalez JE, Long CP, Antoniewicz MR. Comprehensive analysis of glucose

669 and xylose metabolism in *Escherichia coli* under aerobic and anaerobic conditions by

670 13 C metabolic flux analysis. Metab Eng. 2017;39:9-18.

671 19. Legiša M, Kidrič J. Initiation of citric acid accumulation in the early stages of

672 *Aspergillus niger* growth. Appl Microbiol Biot. 1989;31:453-7.

673 20. Akaike H. Information theory and an extension of the maximum likelihood

674 principle. In: Petrov BN, Csáki F. 2nd International Symposium on Information

675 Theory. Budapest: Akadémiai Kiadó; 1973. p. 267–281.

676 21. Capuder M, Šolar T, Benčina M, Legiša M. Highly active, citrate inhibition

677 resistant form of *Aspergillus niger* 6-phosphofructo-1-kinase encoded by a modified

678 pfkA gene. J Biotechnol. 2009;144:51-7.

679 22. De Jongh WA, Nielsen J. Enhanced citrate production through gene insertion in

680 *Aspergillus niger*. Metab Eng. 2008;10:87-96.

681 23. Nishi A. Role of polyphosphate and phospholipid in germinating spores of

682 *Aspergillus niger*. J Bacteriol. 1961;81:10.

683 24. Huson DH, Richter DC, Rausch C, Dezulian T, Franz M, Rupp R. Dendroscope:

684 An interactive viewer for large phylogenetic trees. BMC Bioinformatics. 2007;8:1.

685   25. Ruijter GJ, van de Vondervoort PJ, Visser J. Oxalic acid production by

686   *Aspergillus niger*: an oxalate-non-producing mutant produces citric acid at pH 5 and

687   in the presence of manganese. Microbiology. 1999;145:2569-76.

688   26. Kalisz HM, Hecht HJ, Schomburg D, Schmid RD. Effects of carbohydrate

689   depletion on the structure, stability and activity of glucose oxidase from *Aspergillus*

690   *niger*. BBA-Protein Struct M. 1991;1080:138-142.

691   27. Swoboda BE, Massey V. Purification and properties of the glucose oxidase from

692   *Aspergillus niger*. J Biol Chem. 1965;240:2209-15.

693   28. Wilson R, Turner APF. Glucose oxidase: an ideal enzyme. Biosens Bioelectron.

694   1992;7:165-85.

695   29. Rodríguez H, Fraga R. Phosphate solubilizing bacteria and their role in plant

696   growth promotion. Biotechnol Adv. 1999;17:319-39.

697   30. Chuang CC, Kuo YL, Chao CC, Chao WL. Solubilization of inorganic phosphates

698   and plant growth promotion by *Aspergillus niger*. Biol Fert Soils. 2007;43:575-584.

699   31. Lu H, Cao W, Ouyang L, Xia J, Huang M, Chu J, Zhuang Y, Zhang S, Noorman

700   H. Comprehensive reconstruction and *in silico* analysis of *Aspergillus niger*

701   genome-scale metabolic network model that accounts for 1210 ORFs. Biotechnol

702   Bioeng. 2017;114:685-95.

703   32. Delmas S, Llanos A, Parrou JL, Kokolski M, Pullan ST, Shunburne L, Archer DB.

704   Development of an unmarked gene deletion system for the filamentous fungi

705   *Aspergillus niger* and *Talaromyces versatilis*. Appl Environ Microb. 2014;80:3484-7.

706 **Table 1.** Parameters fitted to our empirical data.

Parameter	Description	Value
$v_{Pe,max}$ (mmol gDW^{-1} h^{-1})	External phosphate maximum input rate[a]	0.08
K_{Pe} (mM)	External phosphate Michaelis constant	0.0333
$v_{P,max}$ (mmol gDW^{-1} h^{-1})	Internal phosphate maximum input rate	0.0008
K_P (mM)	Internal phosphate Michaelis constant	0.0833
v_{G1} (mmol gDW^{-1} h^{-1})	External glucose passive uptake rate	0.00031419 × [GLC][b]
v_{X1} (mmol gDW^{-1} h^{-1})	External xylose passive uptake rate	0.00033 × [XYL][c]
$v_{X2,max}$ (mmol gDW^{-1} h^{-1})	External xylose high-affinity transport maximum rate	0.2
K_{X2} (mM)	External xylose high-affinity transport Michaelis constant	3.33
$v_{X3,max}$ (mmol gDW^{-1} h^{-1})	External xylose low-affinity transport maximum rate	2.5
K_{X3} (mM)	External xylose low-affinity transport Michaelis constant	3.33
[GOX] (mg gDW^{-1})	Concentration of external glucose oxidase enzyme	0.1
v_{CIT} (mmol gDW^{-1} h^{-1})	Citric acid output rate constraint[d]	0.12
v_{OXAL} (mmol gDW^{-1} h^{-1})	Oxalic acid output rate constraint	0.01

707 [a]External phosphate input rate changed 8 hours after the dFBA start time to 0.015 mmol
708 gDW^{-1} h^{-1} if initial pH 2 or 0.004 mmol gDW^{-1} h^{-1} if initial pH 7. [b][GLC] is concentration of
709 external glucose in mM. [c][XYL] is concentration of external xylose in mM. [d]Citric acid output
710 rate constraint changed to 0.016 mmol gDW^{-1} h^{-1} if initial pH above 2.

711

712 **Table 2.** Parameters set to empirical values from the literature.

Parameter	Description	Value	References
$v_{G2,max}$ (mmol gDW^{-1} h^{-1})	External glucose high-affinity transport maximum rate	0.186	[16, 17]
K_{G2} (mM)	External glucose high-affinity transport Michaelis constant	0.26	[16, 17]
K_{i2} (mM)	External glucose high-affinity transport citrate inhibition constant	933	[16, 17]
$v_{G3,max}$ (mmol gDW^{-1} h^{-1})	External glucose low-affinity transport maximum rate	2.706	[16, 17]
K_{G3} (mM)	External glucose low-affinity transport Michaelis constant	3.67	[16, 17]
K_{i3} (mM)	External glucose low-affinity transport citrate inhibition constant	233.21	[16, 17]
$v_{GOX,max}$ (mmol gDW^{-1} h^{-1})	Glucose oxidase (GOX) maximum reaction rate	27.48 × [GOX][a]	[26]
K_{GOX} (mM)	Glucose oxidase (GOX) Michaelis constant	33	[26, 27]

713 [a][GOX] is concentration of external glucose oxidase enzyme in mg gDW^{-1} and was fitted to
714 empirical data (Table 1).

33

Table 3. Acid constants for Equation 10.

Acid species	K_1	K_2	K_3
Citric acid	$10^{-3.128}$	$10^{-4.761}$	$10^{-6.396}$
Gluconic acid	$10^{-3.7}$	0	0
Acetic acid	$10^{-4.757}$	0	0
Malic acid	$10^{-3.459}$	$10^{-5.097}$	0
Succinic acid	$10^{-4.207}$	$10^{-5.636}$	0
Lactic acid	$10^{-3.86}$	0	0
Oxalic acid	$10^{-1.252}$	$10^{-4.266}$	0

Table 4. AIC scores for model selection.

Additional parameters	Number of fitted parameters	AIC score
None	5	438
Nucleic acid component of biomass equation	6	416
Phospholipid component of biomass equation	6	422
Nucleic acid and phospholipid components of biomass equation	7	393
Nucleic acid and phospholipid components of biomass equation, and citric acid output constraint	8	300

721 **Table 5.** Primers used in this work.

Primer	Nucleotide sequence (5' to 3')
pyrG_ex_fw	CTTTGCAGGTGTGGCTGAAC
pyrG_ex_rv	ACAGCAGTGCTTATCTGCGA
oah_up_fw	ACCGCGGTGGCGGCCGCGCTGTGTCCATACCATCAATCC
oah_up_rv	GAATGTTGCAGACAGACAGAAAGCAAAAGAGCAGGCAGTAGTAAGCAAGAAT
oah_down_fw	TCTTTCTTATTCTTGCTTACTACTGCCTGCTCTTTTGCTTTCTGTCTGTCTGC
oah_down_rv	CGGGGGGATCCACTAGTTCTCCTCTTCCCCTGCCTTT
gox_up_fw	ACCGCGGTGGCGGCCGCGAGATGGCAATTTCCGCGAC
gox_up_rv	GAATATTCGAGGATTGTGGGAGAGACAGCGCGTGCAAACTCACCACCAAG
gox_down_fw	CTGTCTTGACCTTGGTGGTGAGTTTGCACGCGCTGTCTCTCCCACAATCC
gox_down_rv	CGGGGGGATCCACTAGTCTACGCTCATGTCCTGGTCC
oah_ex_fw	TAAGGCTACCCAACCCACCC
oah_ex_rv	GCTTATCTAGGCCCCTGCTG
oah_int_fw	ACCCAACCACACCATCCTTC
oah_int_rv	ACCCAGTTCCCCACTAACAC
gox_ex_fw	CACTATCGCCAAGCAGGGAT
gox_ex_rv	AAGGTCTCGTTGAAGGTGGC
gox_int_fw	AGCAACCAGCCTTTCCTCTC
gox_int_rv	CCCAGTTCCAGCCCTCATTT

722

723

35

724 **Figure legends**

725

726 **Figure 1.** Citric acid production commences upon a diauxic growth switch. Empirical

727 data plotted is the mean average of 4 biological replicates and error bars represent

728 standard deviation. Citric acid data are normalised to reflect the amount produced.

729 **A)** Change in biomass dry weight (g/L) over time. **B)** Change in external citric acid

730 concentration (g/L) over time.

731

732 **Figure 2.** Comparing empirical and *in silico* data in response to varying phosphate.

733 Markers represent empirical data and lines represent *in silico* data. Green circles and

734 dashed-dotted lines correspond to 0.05 g/L phosphate. Purple triangles and dashed

735 lines correspond to 0.09 g/L phosphate. Brown squares and solid lines correspond to

736 0.17 g/L phosphate. Empirical data plotted is the mean average of 4 biological

737 replicates and error bars represent standard deviation. Citric acid data are

738 normalised to reflect the amount produced. *In silico* data-points are one per minute.

739 **A)** Change in biomass dry weight (g/L) over time. **B)** Change in external phosphate

740 concentration (g/L) over time. **C)** Change in external citric acid concentration (g/L)

741 over time. **D)** Change in external glucose concentration (g/L) over time.

742

743 **Figure 3.** Simulating citric acid fermentation by dynamic flux balance analysis. A

744 schematic showing the decision process implemented in the dFBA model.

745

746 **Figure 4.** Comparing empirical and *in silico* data in response to different carbon

747 sources. Markers represent empirical data and lines represent *in silico* data. Green

36

748 circles and solid lines correspond to glucose. Purple triangles and dashed lines

749 correspond to xylose. Empirical data plotted is the mean average of 4 biological

750 replicates and error bars represent standard deviation. Citric acid data are

751 normalised to reflect the amount produced. *In silico* data-points are one per minute.

752 **A)** Change in biomass dry weight (g/L) over time. **B)** Change in external phosphate

753 concentration (g/L) over time. **C)** Change in external citric acid concentration (g/L)

754 over time. **D)** Change in external carbon source concentration (g/L) over time.

755

756 **Figure 5.** Change in polyphosphate levels during citric acid fermentation. Empirical

757 data plotted is the mean average of 3 biological replicates and error bars represent

758 standard deviation.

759

760 **Figure 6.** Comparing empirical and *in silico* data in response to Δoah and Δgox

761 knockouts. Markers represent empirical data and lines represent *in silico* data. Green

762 circles and solid lines correspond to Δoah Δgox. Purple triangles and dashed-dotted

763 lines correspond to Δoah. Brown squares and dashed lines correspond to Δgox.

764 Blue diamonds and dotted lines correspond to ΔpyrG control. Empirical data plotted

765 is the mean average of 4 biological replicates and error bars represent standard

766 deviation. Citric acid data are normalised to reflect the amount produced. *In silico*

767 data-points are one per minute. **A)** Change in external citric acid concentration (g/L)

768 over time. **B)** Change in external oxalic acid concentration (g/L) over time. **C)**

769 Change in external gluconic acid concentration (g/L) over time. **D)** Change in

770 external phosphate concentration (g/L) over time.

771   **Table S1.** Biomass equation parameters altered to fit empirical data.

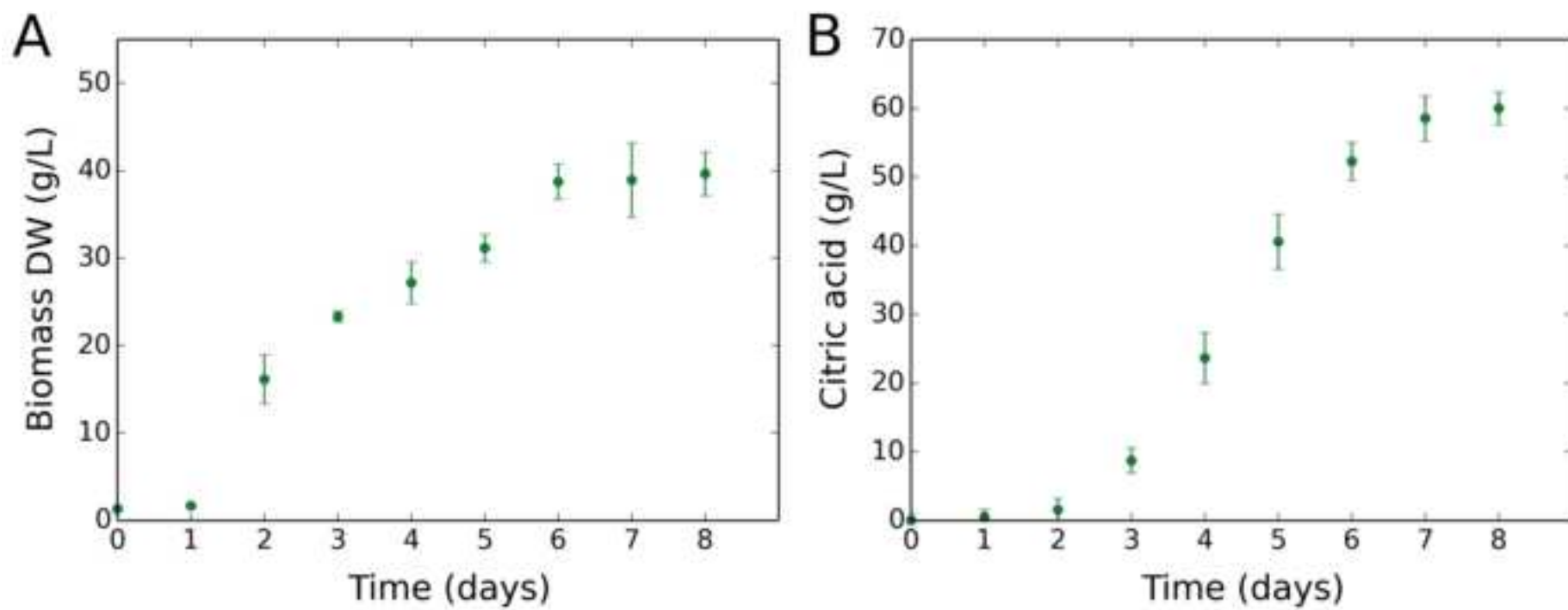| Compound	Before fitting (mmol gDW^{-1} h^{-1})	After fitting (mmol gDW^{-1} h^{-1})
AMP	-0.01402222	-0.0046740733
GMP	-0.01688834	-0.0056294467
CMP	-0.01402222	-0.0046740733
UMP	-0.01117424	-0.0037247467
DAMP	-0.00193736	-0.0006457867
DCMP	-0.00201544	-0.0006718133
DTMP	-0.00193736	-0.0006457867
DGMP	-0.00201544	-0.0006718133
PC	-0.015312	-0.005104
PS	-0.000359	-0.0001196667
PE	-0.034807	-0.0116023333
GL	-0.46	-0.9030928715
ADP	71.60986992	71.5025795733
PI	71.60986992	71.5025795733
ATP	-71.60986992	-71.5025735267
H2O	-69.08036756	-69.0511151733

772

773 **Table S2.** Putative phosphate transporters in ATCC 1015. Top BLASTP hits with

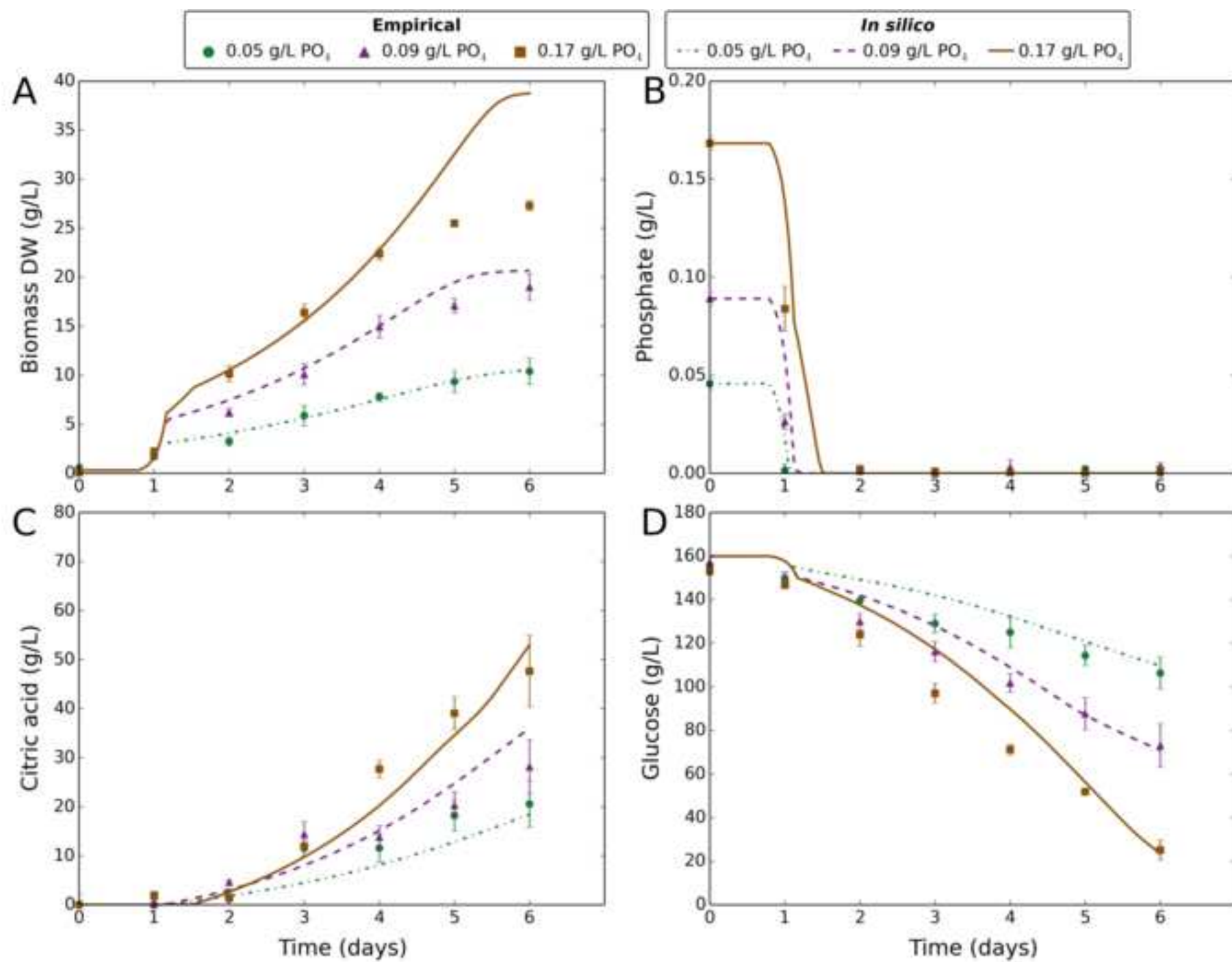774 phosphate transporters in SwissProt database are given.

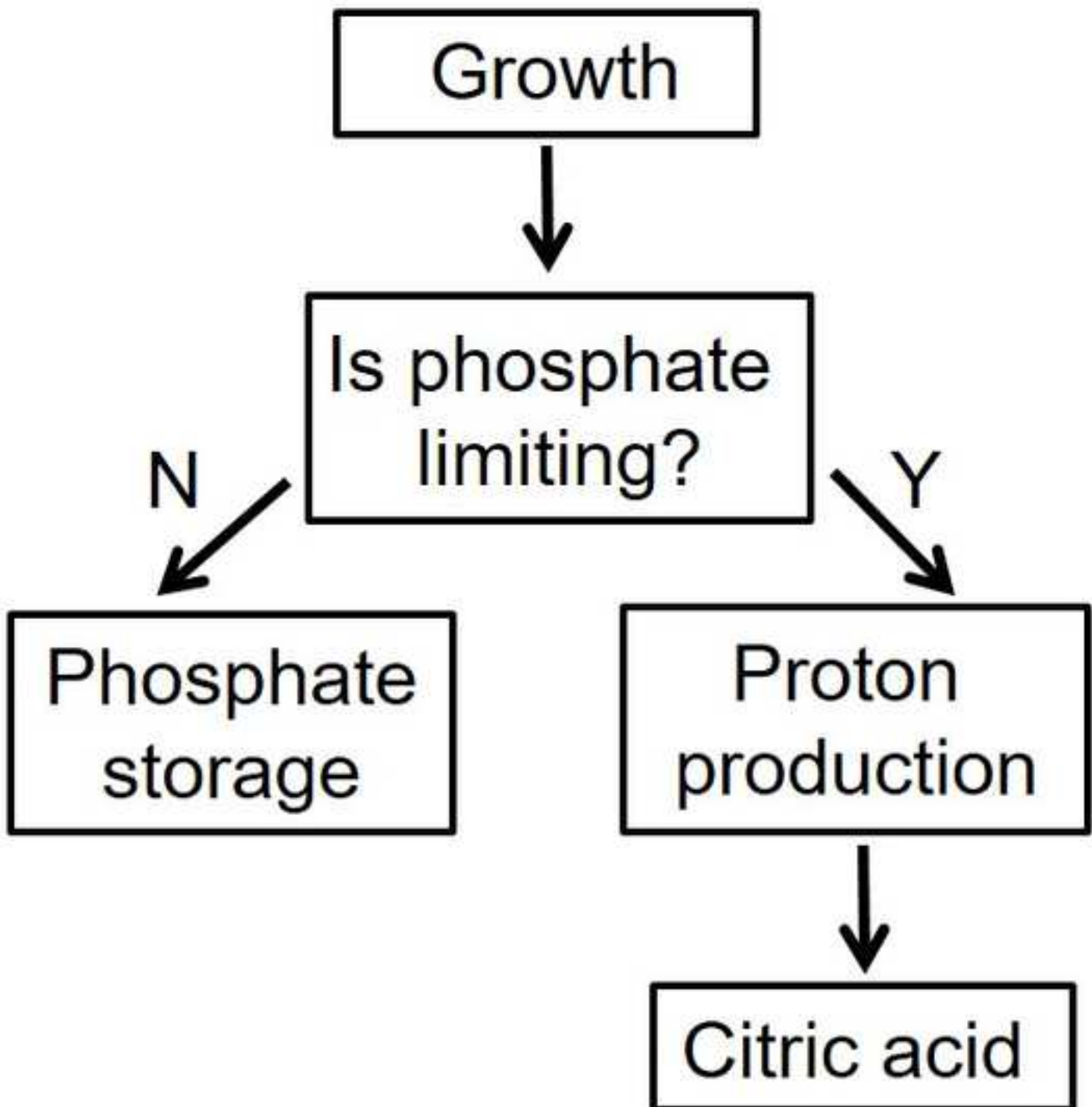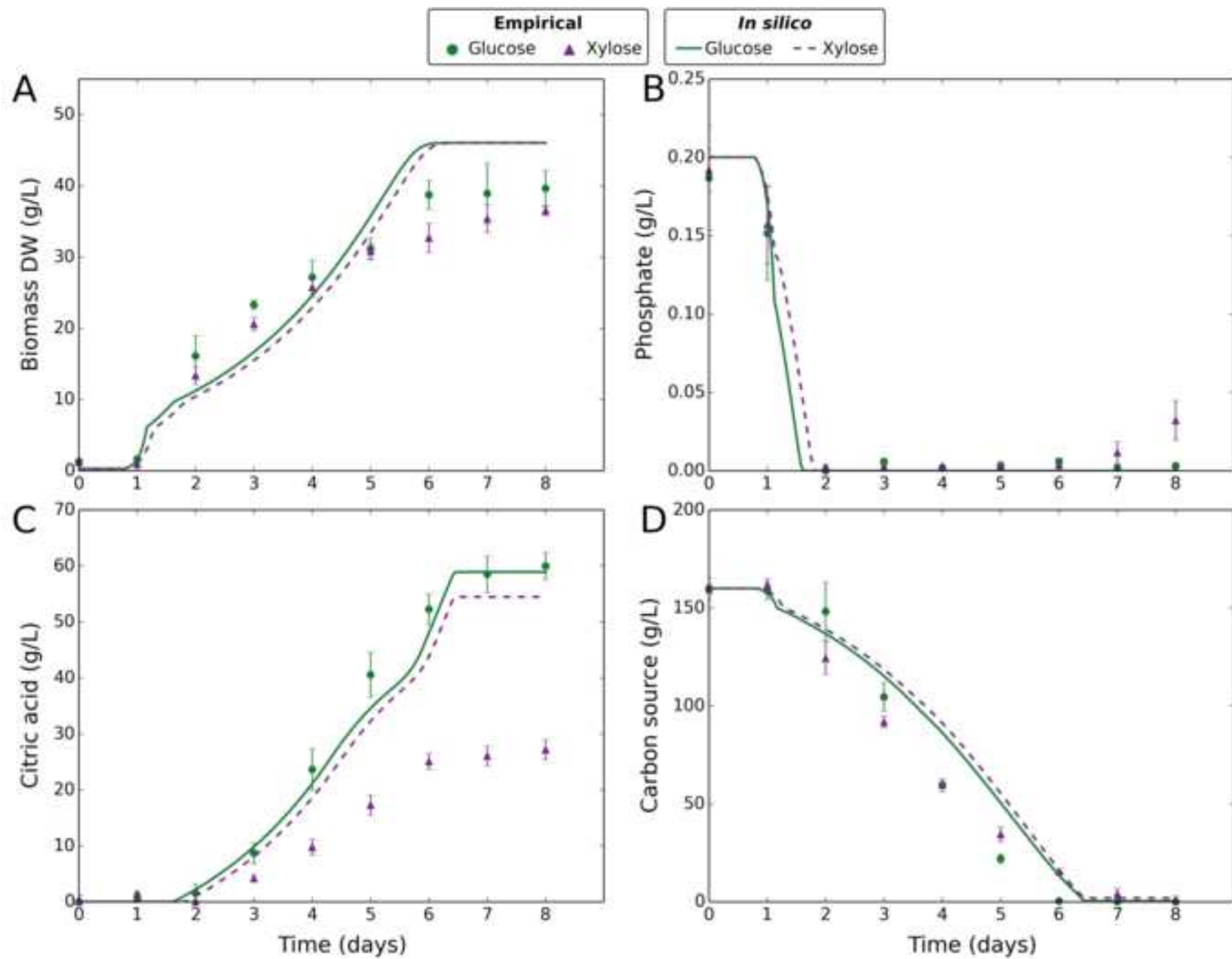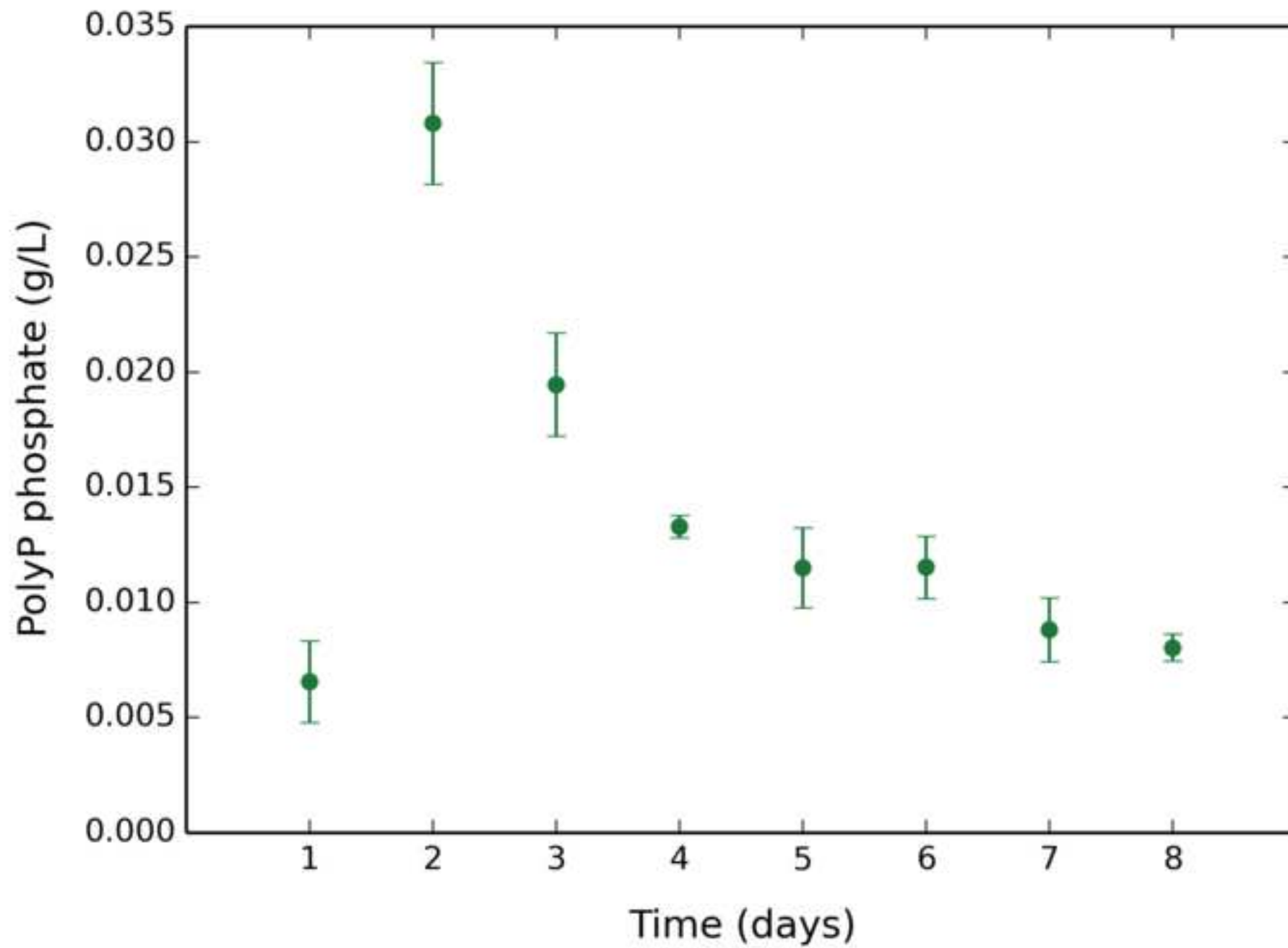| ATCC 1015 locus tag	GenBank accession	Top BLASTP hit (SwissProt)	Identity (%)	E-value
ASPNIDRAFT_173247	EHA22558	P15710.1	37	4e-130
ASPNIDRAFT_190334	EHA20653	P25297.2	34	2e-90
ASPNIDRAFT_121846	EHA27663	Q7RVX9.2	61	0.0
ASPNIDRAFT_52154	EHA22720	O42885.2	29	2e-42
ASPNIDRAFT_42307	EHA25335	Q9S735.1	27	6e-12
ASPNIDRAFT_175394	EHA23128	Q8H074.1	25	2e-26
ASPNIDRAFT_206238	EHA26306	P27514.2	41	0.0
ASPNIDRAFT_35379	EHA27197	Q8H074.1	24	2e-22

775

Supplementary Figure legends

777 **Figure S1.** Phylogenetic tree of putative phosphate transporters in ATCC 1015.

Figure1

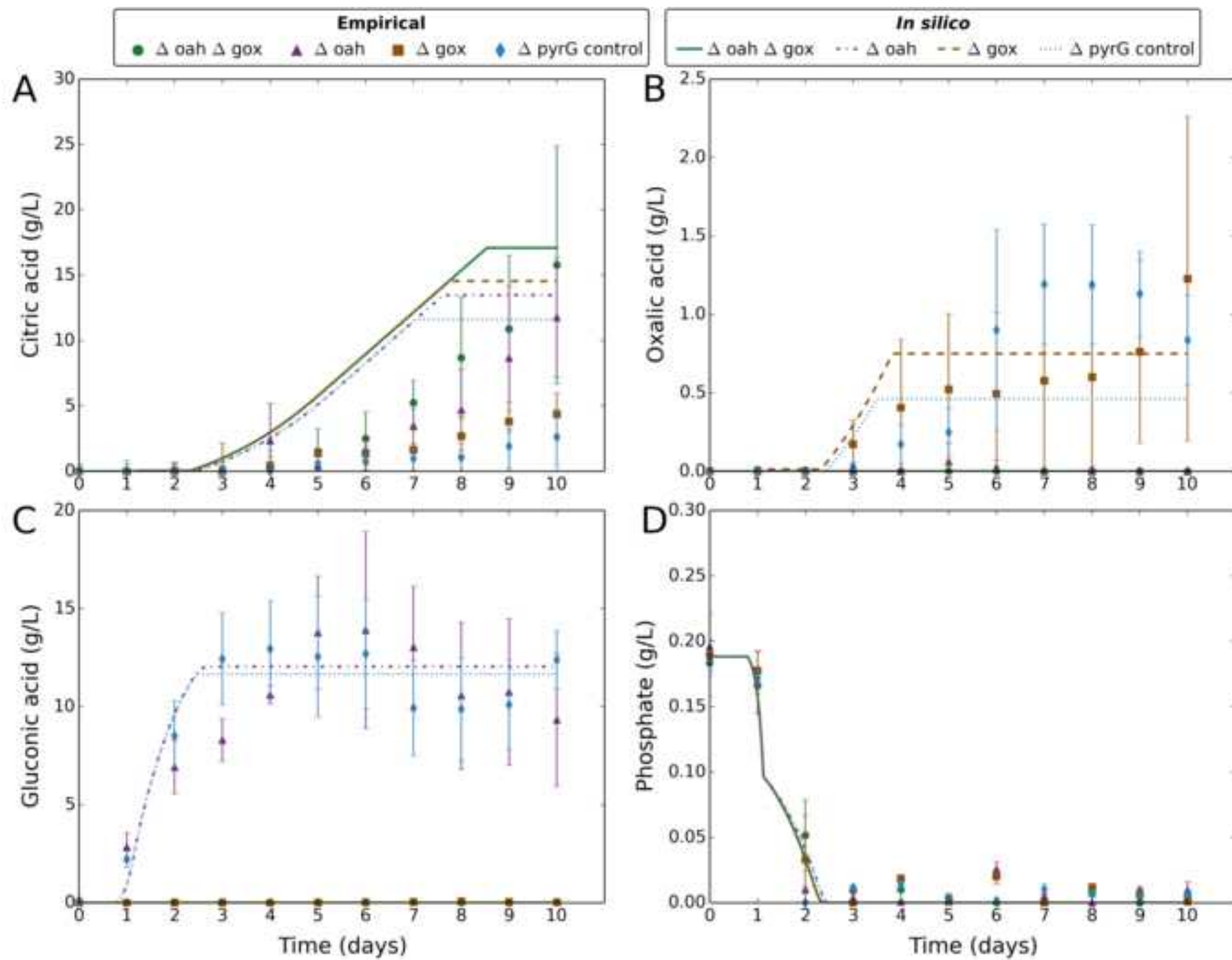Click here to download Figure Figure1.png ⬇

Figure2

Click here to download Figure Figure2.png

Figure3

Figure4

Figure 4

Figure5

Figure6

Click here to download Figure Figure6.png

FigureS1